

pubs.acs.org/JACS Article

Fast Structural Dynamics in Concentrated HCl Solutions: From Proton Hopping to the Bulk Viscosity

Laura Kacenauskaite, Max Moncada Cohen, Stephen J. Van Wyck, and Michael D. Fayer*



Cite This: https://doi.org/10.1021/jacs.3c11620



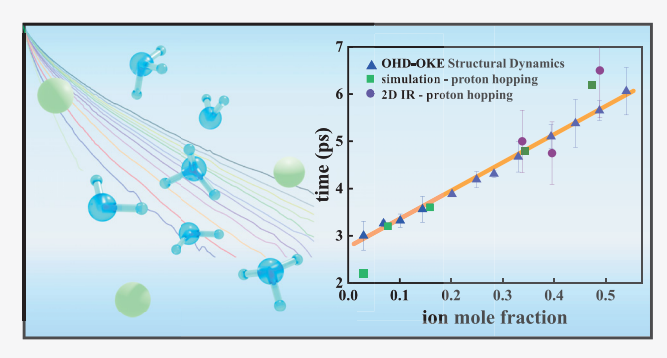
ACCESS

III Metrics & More

Article Recommendations

Supporting Information

ABSTRACT: Concentrated acid solutions, particularly HCl, have been studied extensively to examine the proton hopping and infrared spectral signatures of hydronium ions. Much less attention has been given to the structural dynamics of concentrated HCl solutions. Here, we apply optical heterodyne detected—optical Kerr effect (OHD-OKE) measurements to examine HCl concentration-dependent dynamics from moderate (0.8 m) to very high (15.5 m) concentrations and compare the results to the dynamics of NaCl solutions, as Na⁺ is similar in size to the hydronium cation. Both HCl and NaCl OHD-OKE signals decay as triexponentials at all concentrations, in contrast to pure water, which decays as a biexponential. Two remarkable features of the HCl dynamics are



the following: (1) the bulk viscosity is linearly related to the slowest decay constant, t_3 , and (2) the concentration-dependent proton hopping times, determined by *ab initio* MD simulations and 2D IR chemical exchange experiments, both obtained from the literature, fall on the same line as the slowest structural dynamics relaxation time, t_3 , within experimental error. The structural dynamics of hydronium/chloride/water clusters, with relaxation times t_3 , are responsible for the concentration dependence of microscopic property of proton hopping and the macroscopic bulk viscosity. The slowest time constant (t_3) , which does not have a counterpart in pure water, is 3 ps at 0.8 m and increases by a factor of ~2 by 15.5 m. The two fastest HCl decay constants, t_1 and t_2 , are similar to those of pure water and increase mildly with the concentration.

■ I. INTRODUCTION

Acid solutions have been studied extensively to understand their fundamental nature 1-3 and because of their central roles in technological applications such as water purification, fuel cells, and regeneration of ion exchange resins as well as in the food, textile, metal, and rubber industries.4-7 Since proton diffusion was shown to be the main feature that gives rise to the bulk properties of acid solutions, most of the fundamental research in this area has focused on the properties and dynamics of the proton transfer.⁸⁻¹³ Protons in, e.g., HCl solutions diffuse much faster than small cations in salt solutions, such as NaCl, or water molecules because protons move through the relay mechanism instead of diffusion by the vehicular mechanism associated with metal cations. 14,15 The relay mechanism involves the transfer of a proton from a hydronium cation to an adjacent water molecule. 16 While hydronium also undergoes translational diffusion as the entire cation (vehicular mechanism), fast proton hopping between adjacent water molecules is typically the major contributor to proton transport.17

There has been a great deal of experimental and theoretical research on determining local structures that protons form in water, how a proton is transferred from one water molecule to another, and how to study proton transfer and the structure of the hydrated hydronium cation. ^{17–23} Frequently, experiments

and theory have been directed toward examining concentrated HCl solutions as a model system for their simplicity and importance in industrial applications. Both time-independent measurements including infrared²⁴ and X-ray absorption spectroscopy^{25,26} together with techniques studying proton transfer dynamics, like ultrafast infrared spectroscopy,^{27–29} and theory, including Monte Carlo, density functional, *ab initio* molecular orbital and dynamics simulations,^{9,30–32} have been used to describe structures and parameters that determine the proton transfer mechanism. Though still a subject of extensive debate, these techniques have contributed to developing qualitative and quantitative descriptions of Eigen and Zundel structures of solvated hydronium and time scales of proton displacement as a function of ion concentration.³³

Because of a distinct focus on proton transport in acid solutions, less attention has been directed to studying the overall structural dynamics of the liquid, i.e., the complex,

Received: October 18, 2023 Revised: April 8, 2024 Accepted: April 10, 2024



transient system of solvated hydronium cations, anions, and water molecules. Theoretical models, neutron and X-ray diffraction experiments, ^{25,34–36} X-ray, IR, ³⁷ Raman, and terahertz spectroscopy techniques ^{38–42} have been used to describe concentration-dependent solvation shells around ions semiquantitatively. However, the results vary remarkably, depending on the technique used. These results are especially limited at ion concentrations approaching saturation, where there is insufficient water to ensure complete solvation of individual ions or even ion pairs. ^{43,44} It is generally accepted that the complicated interplay between ions and relatively few water molecules modifies the water hydrogen bonding networks, affects proton hopping, and alters the physicochemical properties of the solutions. However, no detailed quantitative experiments on the dynamics of the microscale structures and their relation to bulk properties or proton hopping have been reported.

Here, we present the results on the structural dynamics of HCl solutions over a broad concentration range using optical heterodyne detected-optical Kerr effect (OHD-OKE) experiments. The OHD-OKE experiment provides the polarizability-polarizability time correlation function, reflecting the collective structural dynamics of the entire HCl solution. OHD-OKE experiments have been previously carried out on moderately concentrated HCl solutions (<3 M) and revealed time scales for structural rearrangement as a function of concentration.⁴⁵ Another study involving OHD-OKE measurements of more concentrated HCl solutions focused on the overall intensity of the signal as a way to quantify the extent of nonspherical symmetry within the sample, i.e., the importance of ordered water molecules in solvation shells and the hydrogen bonding network.⁴⁶ The experiments presented here are conducted on HCl solutions that range from moderately high (0.8 m) to very high (15.5 m) concentrations. Below, we will discuss time scales of the hydronium/chloride/ water network relaxation as a function of ion concentration and demonstrate that the slowest component of the concentration-dependent picosecond time scale structural dynamics of HCl solutions underlies both the macroscopic property of the bulk viscosity and the microscopic property of proton hopping.

For comparison, experiments were also performed on NaCl solutions as Na⁺ is the closest cation in size to hydronium. However, NaCl is not nearly as soluble in water as HCl. Nonetheless, the comparisons show significant differences and similarities between HCl and NaCl solutions at similar concentrations. OHD-OKE experiments on pure water give biexponential decays. 47 Both the HCl and NaCl moderate to high concentration solutions studied here exhibit decays that are triexponentials. The fastest time constants for HCl and NaCl are almost the same as those of pure water at the lowest concentrations and have very mild concentration dependencies. The second time constants have values near that of pure water at the lowest concentrations and become gradually slower with an increasing concentration. The third slowest time constant, t_3 , which has no counterpart in pure water, is particularly interesting. It has a steeper concentration dependence. Simulations from the literature^{25,41} and comparisons to experimental and theoretical studies of LiCl48,49 discussed below suggest that the dynamics with time constant t_3 correspond to structural relaxation of hydronium/chloride/ water clusters and, at the higher concentration, an extended ion/water network.

■ II. EXPERIMENTAL PROCEDURES

A. Sample Preparation. Hydrochloric acid (HCl, 36.5% to 38.0%, w/w), sodium chloride (anhydrous, > 99%), and deionized ultrafiltered water were acquired from Fisher Chemical. All materials were used as received. The sample concentrations were prepared gravimetrically at room temperature. The samples were filtered through a 0.02 μ m filter into a 1 cm path length glass cuvette for higher concentrations, \geq 4 m, and into a 4 cm glass cell for the lower concentrations, <4 m. The cells were sealed with Teflon stoppers. All the experiments were performed in a temperature-controlled room at 24.4 °C with a tolerance of \pm 0.1 °C.

The HCl concentration range studied was 0.8 to 15.5 m. These molalities correspond to ion mole fractions (IMF) from 0.03 to 0.54, as one HCl molecule corresponds to two ions. However, when HCl is added to water, one water associates with a proton to form a hydronium. Therefore, the number of water molecules is n-1, where n is the number of water molecules added to form the solution. Thus, for 1 HCl per 10 water molecules, the IMF is 2/11 = 0.18 (note that for NaCl, it will be 2/12 = 0.17).

Bulk viscosity values of HCl and NaCl solutions used in this paper were obtained from the literature. 50,51

B. Optical Heterodyne Detected-Optical Kerr Effect Experimental Setup. The OHD-OKE experiment is a nonresonant pump-probe experiment with a strong pump and a weak probe pulse. The electric field of the pump induces an oscillating macroscopic polarization along a direction determined by the local anisotropic polarizability of the ion/water structures. The induced oscillating dipoles of the local structures couple to the pump pulse's electric field and produce a minute structural modification, resulting in a small shift of the polarizability toward the direction of the pump's electric field. The alignment causes a small transient birefringence in the sample, which decays due to the dynamical relaxation and eventual randomization of the ion/water structures. The resulting signal, 52-56 following integration, yields the polarizability-polarizability correlation function. Linear response theory⁵⁷ states that a system, initially in thermal equilibrium, will relax from a small perturbation by the system's thermal equilibrium fluctuations. Therefore, the timedependent polarizability-polarizability correlation function, measured using the OHD-OKE technique, provides the thermal equilibrium structural dynamics of the HCl and NaCl aqueous solutions.

The OHD-OKE experimental system has been described in detail previously. 58,59 Briefly, ultrafast pulses were generated by a 90 MHz Ti:sapphire oscillator, which was used to seed a 5 kHz Ti:sapphire regenerative amplifier. The pulse duration was adjusted to be ~200 fs for the shorter time data and 2.5 ps (fwhm) for the longer time data using a linear chirped pulse compressor. Using longer pulses for the slower decaying portions of the data improved the signal-to-noise ratio. The intense pump and weaker probe pulse were produced by using a 98%/2% beam splitter. The linearly polarized pump pulse introduced a transient birefringence along the axis of its electric field vector. The weaker probe pulse, with the polarization set at 45° relative to the pump pulse, was used to measure the birefringence. The probe was passed through crossed polarizers, one before and one after the sample. The pump-pulse-induced birefringence causes depolarization of the probe pulse, resulting in some transmission through the second polarizer. As structural relaxation occurs in the sample, the birefringence decays, and transmission through the second polarizer decreases. Therefore, the time dependence of the depolarization caused by the pump pulse is measured.

To improve the signal-to-noise ratio and reduce the interference of scattered pump light with the signal, heterodyne detection with phase and polarization cycling was used. ⁶⁰ The total phase and polarization cycling was a four-shot sequence repeating at 1.25 kHz. A balanced detector pair was used with a reference pulse going into one photodiode and the probe/signal pulse going into the other. The difference between the two signals was amplified. The reference pulse amplitude was adjusted to almost eliminate the local oscillator intensity of the heterodyned probe/signal pulse, leaving mainly the heterodyned signal. The heterodyned signal was measured with a

lock-in amplifier at a modulation frequency of 1.25 kHz. The timing of the probe pulse was scanned with a computer-controlled delay stage. The pump intensity was reduced until no dependence on the pump power was observed in the recorded data.

■ III. RESULTS AND DISCUSSION

A. HCl Solutions. Figure 1 displays some of the OHD-OKE signal decay curves taken on pure water and HCl

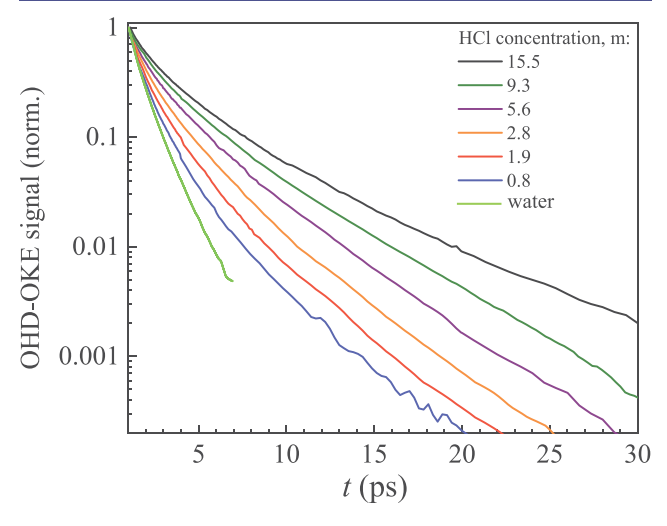


Figure 1. Selected OHD-OKE signal decays of moderate to high concentration HCl solutions and decay of pure water. The decays are normalized at 1 ps. The complete set of decays is shown in Figure S1.

solutions as a function of concentration. The complete set of decay curves, measured over the concentration range from 0.8 to 15.5 m (IMF from 0.03 to 0.54), is shown in the Supporting Information (SI), Figure S1. The amplitudes of the decays can be observed over three to four orders of magnitude except for pure water, which produces a much weaker signal than the HCl solutions due to its smaller anisotropic polarizability. As the ion concentration is increased, the signal intensity also increased.

The OHD-OKE data for HCl solutions at all concentrations studied fit well to triexponential decay functions:

$$r(t) = R'(t)$$

$$= A_1 \exp(-t/t_1) + A_2 \exp(-t/t_2) + A_3 \exp(-t/t_3)$$
(1)

where R'(t) is the decaying OHD-OKE signal (the time derivative of the polarizability-polarizability correlation function), the t_i 's are the decay time constants, and A_i 's are the associated amplitudes. The integration of eq 1 gives the polarizability-polarizability correlation:

$$R(t) = A_1 t_1 \exp(-t/t_1) + A_2 t_2 \exp(-t/t_2)$$

$$+ A_3 t_3 \exp(-t/t_3)$$
(2)

Because the sign of the signal in the experiments is arbitrary, we take R(t) to be positive. The prefactors in eq 2 can be normalized and relabeled in the following manner:

$$C_{1} = \frac{A_{1}t_{1}}{A_{1}t_{1} + A_{2}t_{2} + A_{3}t_{3}}$$

$$C_{2} = \frac{A_{2}t_{2}}{A_{1}t_{1} + A_{2}t_{2} + A_{3}t_{3}}$$

$$C_{3} = \frac{A_{3}t_{3}}{A_{1}t_{1} + A_{2}t_{2} + A_{3}t_{3}}$$
(3)

The C_i 's sum to 1 and represent the fractional amplitudes, i.e., the normalized relative fractions associated with each time component.

Figure 2 shows the decay time constants t_1 , t_2 , and t_3 , obtained from the OHD-OKE signal decays of HCl solutions

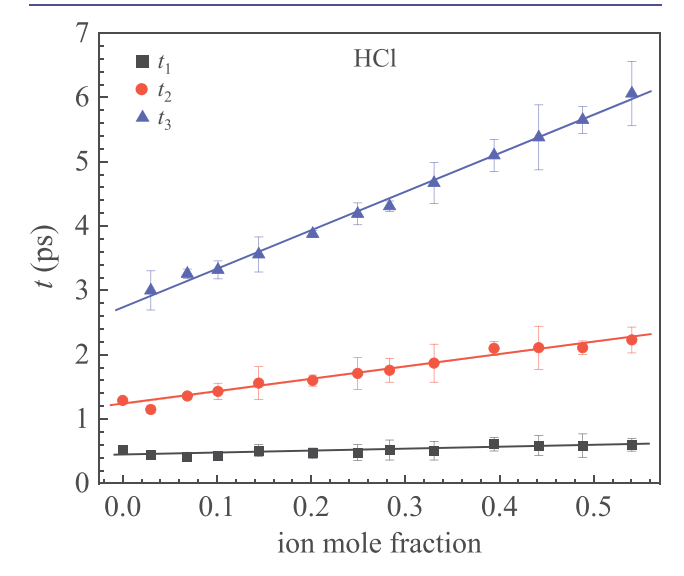


Figure 2. Time constants obtained from the triexponential decay fits to the OHD-OKE signal decays of HCl solutions at different concentrations (ion mole fractions).

as a function of the ion mole fraction. The pure water OHD-OKE signal decays as a biexponential, with $t_1 = 0.52$ and $t_2 = 1.3$ ps. The value of t_1 in the HCl solutions increases to only 0.6 ps at the highest acid concentration. The black line through the data is a linear fit with a slope of only 0.31 ± 0.06 ps/IMF. t_2 has a mild slope of 1.94 ± 0.1 ps/IMF and increases by ~ 1 ps over the same concentration range. t_3 , which does not occur in pure water, has a significantly larger slope of 5.95 ± 0.1 ps/IMF, ~ 3 times greater than that of t_2 , and increases by ~ 3 ps from IMF = 0.03 to 0.54.

A recent OHD-OKE study of the concentration-dependent dynamics in aqueous LiCl solutions for moderate to very high concentrations found that the solutions also had two fast components closely related to those of pure water. The fastest, t_1 , had a pure water value of ~ 0.5 ps, which was almost constant across a wide concentration range within experimental error. t_2 had a pure water value of ~ 1.3 ps at the lowest concentrations studied, which increased gradually with increasing concentration. The HCl and NaCl (discussed below) solutions studied here showed similar behavior. Comparison of the experimental LiCl data to structural simulations from the literature showed that the two fast decay components correspond to the dynamics related to solvated Li⁺/Cl⁻ contact ion pairs. In contrast, the slow components, which are not present in pure water, are

associated with the dynamics of large ion—water clusters and the extended ion/water network. The slowest component of the LiCl OHD-OKE decay data has a slope of 29 ps/IMF, which is much greater than that of HCl and almost identical to that of NaCl, as discussed below.

Equation 3 gives the normalized fractional amplitudes of the time components of the polarizability—polarizability time correlation function. In Figure 3, the coefficients are plotted

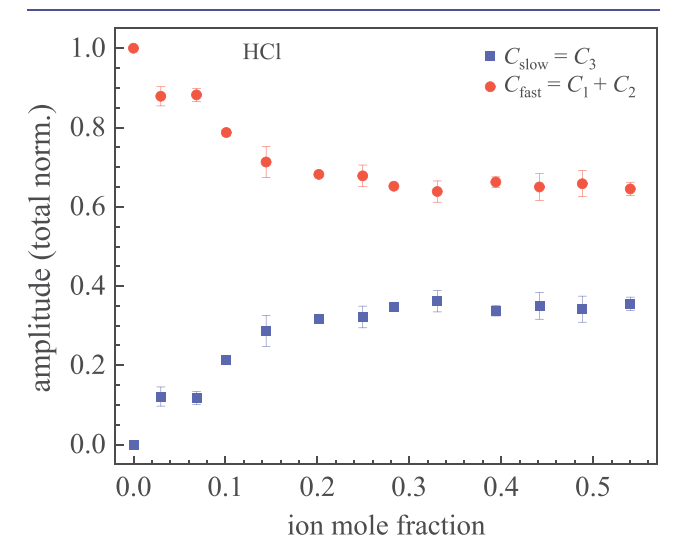


Figure 3. Fractional amplitudes obtained from the triexponential decay fits to the OHD-OKE signal decays of HCl solutions at different concentrations (ion mole fractions). $C_{\rm fast} = C_1 + C_2$, the sum of the amplitudes of the two fastest decay components. $C_{\rm slow} = C_3$, the amplitude of the slowest decay component.

in the following manner. $C_{\rm fast} = C_1 + C_2$ reflects the fraction of the total decay that is water-like in the sense that in the limit of IMF = 0, $C_{\rm fast} = 1$, i.e., only t_1 and t_2 exist in pure water. The slower dynamics, which are not present in pure water, are $C_{\rm slow} = C_3$ (see Figure S2 for plots of C_1 , C_2 , and C_3 individually).

This type of grouping was found to be very useful in analyzing the LiCl data and for comparison to simulations. As the HCl IMF increases, the relative fractions of the decay that are $C_{\rm fast}$ decrease and $C_{\rm slow}$ increase. However, at IMF = ~0.2, the trend changes. $C_{\rm fast}$ and $C_{\rm slow}$ stop changing (plateau) with increasing IMF within experimental error. The plateaus do not imply that the *numbers* of ion/water structures that give rise to the fast $(t_1$ and $t_2)$ and slow (t_3) dynamics with coefficients $C_{\rm fast}$ and $C_{\rm slow}$ are constant with increasing IMF. The plateaus only show that the *ratio* of the $C_{\rm fast}$ and $C_{\rm slow}$ amplitudes of the components of the polarizability-polarizability time correlation function is not changing with concentration.

To understand these results qualitatively, it is useful to think about structural changes within the sample as the concentration of the acid increases. Only at the lowest IMFs studied are there some water molecules that can be considered to be like those in pure water. At the lowest HCl concentration studied (IMF = 0.03), there are $n = \sim 67$ water molecules per hydronium/chloride pair. This number is sufficient to solvate the ions and have water—water hydrogen bonding configurations that do not include ions and are outside the ion first solvation shell. For IMF = 0.2, n = 9. It takes 6-8 hydroxyls to solvate an isolated Cl⁻ and three water molecules to solvate an isolated hydronium.

like configurations will not be possible, as the lack of solvating water molecules will result in an extended network of ions and shared water molecules with a variety of hydronium/chloride/water local cluster configurations.

The IMF range over which $C_{\rm fast}$ decreases and $C_{\rm slow}$ increases (with the slopes of $\mp 1.5 \pm 0.2$ au/IMF) is the range where there are sufficient water molecules to have some groupings that are like pure water, but these vanish as the IMF increases. The plateaus shown in Figure 3, i.e., constant $C_{\rm fast}/C_{\rm slow}$, are not found in experiments on LiCl. There, as the LiCl IMF increases, both $C_{\rm fast}$ and $C_{\rm slow}$ change linearly (with slopes of $\mp 1.48 \pm 0.01$ au/IMF) over the entire LiCl concentration range of IMF from 0.06 to 0.38 that was studied. This concentration range encompasses the region where HCl $C_{\rm fast}$ and $C_{\rm slow}$ become independent of the IMF.

For LiCl, it was shown by comparison to simulations that $C_{\rm fast}$ is associated with solvated contact ion pairs, and $C_{\rm slow}$ is related to large ion/water clusters. ^{48,49} If this correlation between the LiCl $C_{\rm fast}$ and $C_{\rm slow}$ structures also applies to HCl, then the initial HCl slopes, which for IMF < 0.2 are very similar to the corresponding slopes in LiCl solutions, would indicate a decrease in solvated hydronium/Cl⁻ ion pairs and an increase in larger hydronium/chloride/water clusters. At higher IMFs, the clusters would form a continuous ion/water network as there are too few water molecules to separate one cluster from another. The clusters would have different local structures. Both the fast and slow dynamics become slower with increasing concentration (see Figure 2), indicating that the forms of the cluster structures are changing.

The nature of species in HCl solutions at moderate to high concentrations has been studied experimentally and theoretically by using various techniques. Recent high level density functional theory molecular dynamics simulations have been applied to a wide range of HCl concentrations from 2.5 m $(IMF = \sim 0.1)$ to 16 m $(IMF = \sim 0.56)$. This concentration range is similar to that studied here. The simulations were combined with X-ray absorption fine structure experiments (MD-EXAFS) to provide a detailed depiction of HCl concentration-dependent solution structures. 25,41 In addition, terahertz spectroscopy has been used extensively to uncover the signatures of ion pairing in concentrated salt solutions. The works of Havenith and co-workers provided evidence that chloride anions tend to form ion pairs in salts and acids, especially as the concentration increases. 38,39 Most chloride and hydronium ions form contact ion pairs (Cl-·H₃O+) at higher concentrations.⁶³ The presence of contact ion pairs is smaller but still significant at lower concentrations, e.g., 2.5 m (~0.1 IMF). A recent study by Voth and co-workers⁶⁴ showed that chloride ions posed an entropic barrier to proton hopping that increases with greater HCl concentration. At higher HCl concentrations, the relay mechanism of proton diffusion was shown to be suppressed by the presence of chloride ions forming contact ion pairs, with protons instead fluctuating between adjacent waters. These simulation results are consistent with the discussion of Figure 3, given above, in which, within the nonplateau range of IMF < 0.2, there are sufficient water molecules to form solvation shells for ions and contact ion pairs. However, at the higher concentrations, there are insufficient water molecules to give rise to a significant number of solvent-separated ion pairs or small ion/water clusters separated from each other by water. Therefore, at high concentrations, IMF > 0.2, it is more appropriate to view the solution as consisting of large hydronium/Cl⁻/water clusters that are locally varied in structure and form a continuous ion/water network, as in the description of highly concentrated LiCl solutions.

B. NaCl Solutions. To distinguish the effects of proton transfer in the OHD-OKE data of the HCl solutions, NaCl solutions were investigated over a concentration range up to the limit of saturation (IMF = 0.18). Na⁺ is similar in size to a hydronium cation. The OHD-OKE signals of NaCl solutions also decay as triexponential functions at all concentrations studied, as shown in SI Figure S3. The three time constants as a function of NaCl IMF are shown in Figure 4. The lines

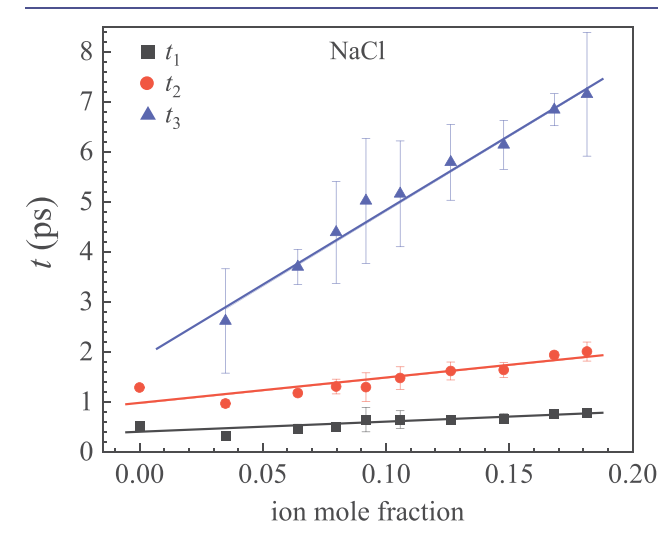


Figure 4. Time constants obtained from the triexponential decay fits to the decays of the OHD-OKE signal of NaCl solutions at different concentrations (ion mole fractions).

through the data are linear fits with slopes of 2.1 ± 0.5 , 5.1 ± 0.9 , and 30 ± 1.6 ps/IMF for t_1 , t_2 , and t_3 , respectively. These slopes are much steeper than the corresponding HCl slopes and comparable to those in LiCl solutions. The t_3 values for NaCl at the lowest and highest concentrations studied are 2.9 (IMF = 0.03) and 7.2 ps (IMF = 0.18). In contrast to HCl, t_3 in NaCl solutions changes significantly over a relatively small concentration range.

The NaCl concentration dependencies of the correlation time fractional amplitudes, $C_{\text{fast}} = C_1 + C_2$ and $C_{\text{slow}} = C_3$, are shown in Figure S5. Individual amplitudes of all components can be found in Figure S4. The lines through the data are linear fits with the C_{fast} slope equal to -0.43 ± 0.04 au/IMF, and the C_{slow} slope is the same with the opposite sign. Unlike the equivalent data for HCl shown in Figure 3, where C_{fast} and C_{slow} decay to plateaus, the corresponding amplitudes in NaCl solutions continue to decay monotonically over the limited concentration range studied. The initial decays of the HCl amplitudes cover about the same range as the total NaCl data. Over this range, the HCl slopes are ±1.5 au/IMF, roughly 3fold greater than those of NaCl. Even though t_3 becomes substantially longer with increasing concentration of NaCl (Figure 4), the fraction of the dynamics that has the t_3 time constant (C_{slow}) increases very little (Figure S5), 7%, over the concentration range, which approaches the solubility limit. In contrast to the LiCl⁴⁸ or HCl, which, as discussed above, tend to form contact ion pairs even at the lower ends of the concentration ranges studied, it has been shown that NaCl almost exclusively forms water-separated ion pairs. 65 As the concentration increases, the number of water separated Na⁺/Cl⁻ pairs increases. This growth in water-separated ion pairs may be responsible for the lengthening of t_1 and t_2 , but they do not contribute to $C_{\rm slow}$. As the concentration approaches the solubility limit of 10 water molecules per ion pair (IMF = 0.18), it becomes difficult to form water-separated ion pairs that are fully isolated from each other by water molecules. A small fraction of contact ion pairs (not water-separated) and larger clusters form, giving rise to the amplitude of $C_{\rm slow}$. At just above an IMF of 0.18, it is possible that the clustering of contact ion pairs cannot be supported in solution, leading to crystallization.

C. Bulk Viscosity. The differences between salt and HCl solutions are also evident from their concentration-dependent viscosities. Figure 5 shows the concentration dependencies of

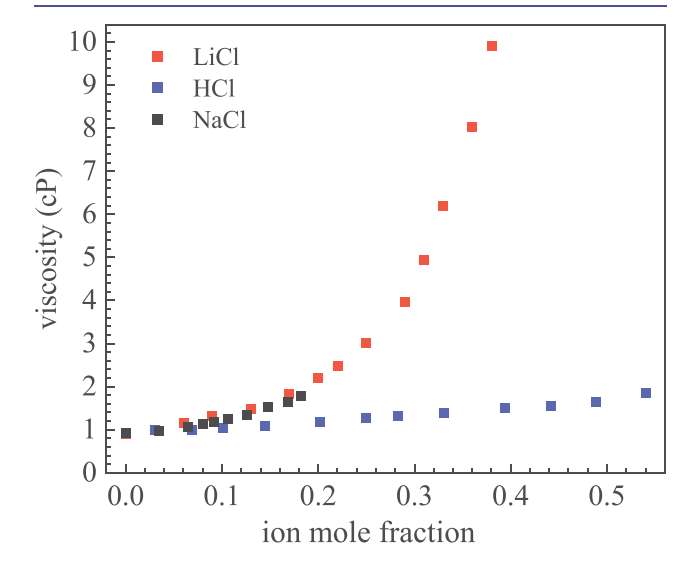


Figure 5. Viscosity of aqueous LiCl, HCl, and NaCl solutions as a function of salt/acid concentration (ion mole fraction). Values are obtained from Mao et al.,⁶⁶ Nishikata et al.,⁵⁰ and Ozbek et al.,⁵¹ respectively.

the viscosities of the HCl, NaCl, and LiCl solutions. The viscosity of HCl is essentially linear with respect to the IMF. NaCl has a much greater increase in viscosity over the accessible range up to IMF = \sim 0.18, just below its solubility limit. The comparatively low solubility of NaCl does not cause the difference between HCl and NaCl. LiCl is soluble to a much higher concentration, and NaCl follows the same trend at lower concentrations. The concentration-dependent viscosities of the salts and HCl have very different functional forms.

Recent OHD-OKE studies found that the bulk viscosities of LiCl and LiBr 48 solutions are linearly related to the correlation time of the slow decay components of the polarizability—polarizability time correlation function, defined as the weighted sum of the time constants not present in pure water. Here solutions were investigated, and the temperature dependences of LiCl and LiBr solutions were investigated, and the temperature dependences of two concentrations of LiCl were studied. Similar to NaCl studied here, the two fast decays, t_1 and t_2 , were water-like in the sense that their values approached the water values when the concentration went to zero and they did not change a great deal with concentration. However, for the LiCl and LiBr systems, two slow time constants $(t_3$ and $t_4)$ were not present

in bulk water. These four components of the polarizability-polarizability time correlation function were divided into two groups: $C_{\rm Fast}$ and $C_{\rm Slow}$. With the slow correlation time defined as $\tau_{\rm C}^{\rm slow} = C_3 t_3 + C_4 t_4$. The $\tau_{\rm C}^{\rm slow}$ concentration dependences and the two temperature dependences all showed a linear correlation with the viscosities. Moreover, all four sets of viscosity vs $\tau_{\rm C}^{\rm slow}$ points fell on the same line. For LiCl concentration dependence, comparison to simulations from the literature showed that $C_{\rm Slow}$ and therefore, t_3 and t_4 arose from the dynamics of large ion/water clusters. The simulations showed that the clusters increase in size with an increasing concentration.

For NaCl OHD-OKE decays, the slow correlation time is defined as $\tau_C^{\rm slow} = C_3 t_3$; there is only one slow component. The relationship between the NaCl viscosity and $\tau_C^{\rm slow}$ is shown in Figure 6. Like LiCl and LiBr, the viscosity of NaCl is directly

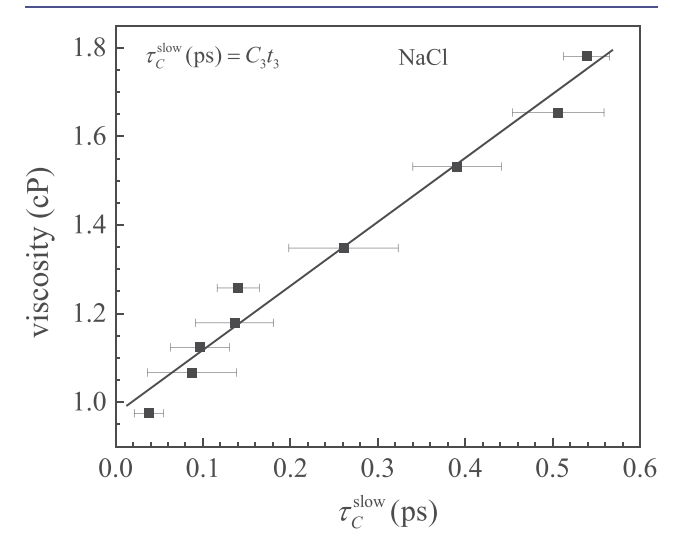


Figure 6. Viscosity of NaCl solutions as a function of the correlation time. Viscosities were obtained from Ozbek et al. ⁵¹ The black line is a linear fit to the data.

proportional to τ_C^{slow} , which shows that the increase in viscosity with increasing concentration is determined by the rise in the relative fraction of the slow dynamics, C_3 , and the increase in the corresponding time constant, t_3 .

Figure 5 shows that the concentration dependence of the viscosity of HCl is very different from that of NaCl and LiCl. (Figure S6 shows a plot of the HCl viscosity vs concentration.) In contrast to the salt solutions, the linear relationship between $\tau_C^{\rm slow}$ and the HCl viscosity does not hold (see Figure S7). However, there is a direct relationship between the HCl solution viscosity and its dynamics, as shown in Figure 7. The bulk viscosity is linearly dependent on t_3 alone (see Figure 2) over the entire HCl concentration range studied rather than a correlation time $\tau_C^{\text{slow}} = C_3 t_3$. The relation holds at the lower concentrations where C_3 is increasing with concentration and at the higher concentrations where C_3 is independent of concentration. The viscosity of HCl solutions is determined by the structural dynamics of the hydronium/Cl⁻/water configurations that relax with time constant t_3 , independent of the fraction of the dynamics that relax on faster time scales.

D. Proton Hopping. The experiments show that a bulk property, viscosity, is linearly correlated with the slowest hydronium/ Cl^- /water relaxation time, t_3 . One of the most important features of HCl solutions and acids in general is

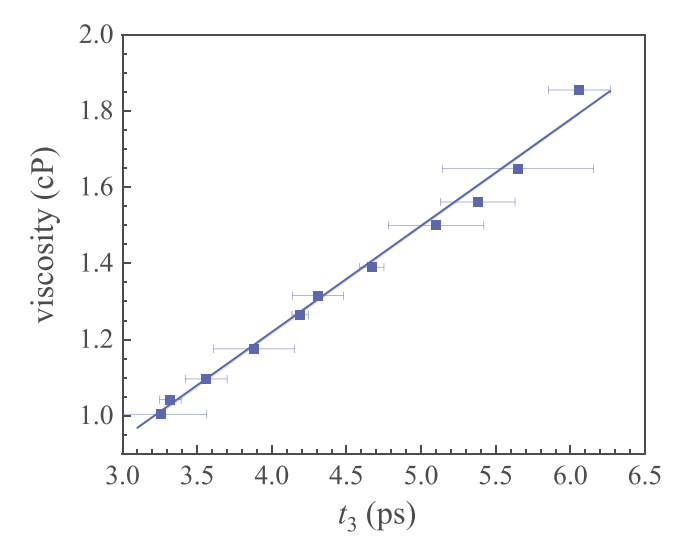


Figure 7. Viscosity of HCl solutions plotted as a function of the slowest decay time component, t_3 . The blue line is a linear fit to the data.

proton hopping. Fast proton diffusion in acid solutions occurs via the relay mechanism. A hydronium proton transfers to a hydrogen-bonded water molecule. Following the proton hop, the original hydronium becomes a water molecule and the water molecule that received the proton becomes a hydronium. In acid solutions, the proton mainly moves without the necessity of physical diffusion of the entire cation, in contrast to the vehicular mechanism, which is the sole mechanism in salt solutions. 69

The three hydrogens in hydronium that are bound to an oxygen are only weakly bound. Any one of them can hop to an H-bonded water molecule. Because the potential energy well for the position of each hydrogen is shallow, the hydrogens rapidly fluctuate about their average bound positions due to thermal fluctuations of the surrounding medium. A sufficiently large fluctuation of one of the hydrogen's potentials will raise its energy and lower the energy for the hydrogen to be bound to an adjacent H-bonded oxygen, resulting in a proton hop. For hydronium in water at very low concentration, there is evidence that the same H-bond network rearrangements that occur in pure water produce the potential fluctuations that induce proton hopping.²⁷

Figure 8 displays time constants for three distinct types of data vs IMF. The purple circles are direct ultrafast 2D IR chemical exchange spectroscopy measurements of the proton hopping time in concentrated HCl.²⁷ The green squares are the results of ab initio molecular dynamics simulations of proton hopping in concentrated HCl.²⁷ (Note that there are no error bars for the simulated proton hopping time constants.) The blue triangles are the t_3 values measured with the OHD-OKE experiments (see Figure 2). The orange line is the linear fit to the t_3 values, the same line as that shown in Figure 2. Although there is scatter in the various types of data, Figure 8 provides evidence that the concentrationdependent proton hopping time is the same as t_3 , the slowest time constant for the hydronium/Cl⁻/water structural relaxation. As discussed further below, the data in Figure 8 indicate that structural relaxation with time constant t_3 is responsible for the potential fluctuations that cause proton hopping.

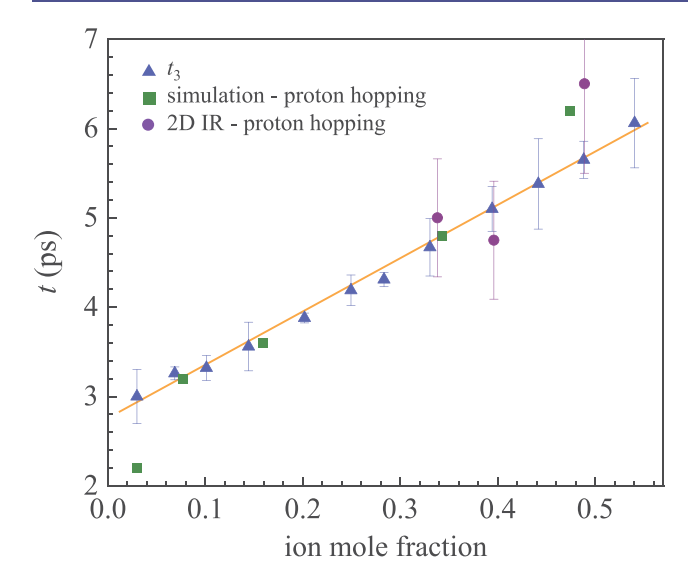


Figure 8. Slowest decay time component from OHD-OKE data of HCl solutions, t_3 , and proton hopping times from *ab initio* molecular dynamics simulations and 2D IR measurements plotted as a function of the HCl concentration (ion mole fraction).²⁷

The fastest decay component, t_1 (see Figure 2), is ~0.5 ps and changes very little over the entire concentration range. 2D IR experiments on pure water have a 0.4 ± 0.1 ps decay component that, simulations show, is caused by very local Hbond fluctuations, mainly in O-H bond lengths. 70,71 2D IR and OHD-OKE measure different time correlation functions. If both measure the structural dynamics of the same process, the time constants would be expected to be similar. Then, the data suggest that t_1 reflects H-bond length fluctuations. The 2D IR measurements also have a slower component of 1.7 ± 0.3 ps that simulations show involves the rearrangements of the Hbond network in pure water. Likewise, in the OHD-OKE experiments, t_2 is 1.3 \pm 0.2 ps in pure water. It slows with an increasing HCl concentration to \sim 2.3 ps. It is possible that t_2 is also caused by water H-bond rearrangements that slow with the increasing presence of hydronium and Cl⁻. However, as shown in Figure 2, neither t_1 nor t_2 track the proton hopping experiments or simulations. As discussed above, t_3 has no counterpart in pure water and involves hydronium/Cl⁻/water cluster structural fluctuation. As the HCl concentration (IMF) increases, t_3 , the 2D IR proton hopping experiments, and the ab initio MD simulations display the same dependence on the IMF, within error.

E. Proton Hopping, Bulk Viscosity, and the Slowest Time Constant, t_3 . Structural relaxation with the time constant t_3 plays a central role in the properties of concentrated HCl solutions. The novel observation in this study is that the t_3 structural relaxation was shown to underlie the macroscopic bulk viscosity (Figure 7) and microscopic proton hopping (Figure 8). An important question that needs to be addressed is whether the OHD-OKE method directly observes the proton hopping time as t_3 , or does t_3 reflect the structural relaxation that induces proton hopping? To answer this question, the relationship of t_3 to proton hopping and bulk viscosity is considered below.

The polarizability anisotropies of a hydronium cation and a water molecule will differ. When a proton hops, the local direction of the principal axis of the polarizability anisotropy can change. Figure 8 indicates that the proton hopping time

and t_3 are the same over a wide range of concentrations, perhaps indicating that t_3 is a direct measure of the proton hopping time. The alternate explanation is that t_3 is the time scale for structural relaxation of hydronium/chloride/water clusters that generate the fluctuating potentials that induce proton hopping.

Another consideration that favors structural relaxation driving proton hopping is the source of the OHD-OKE signal. The local hydronium, chloride, and water structures will constantly undergo fluctuations involving translational and orientational motions. These can be viewed as a random walk in the structure configuration space. The local structures (clusters) have anisotropic polarizability. The electric field of the pump pulse couples to this anisotropic polarizability, skewing the random walk, causing the principal axis of the local polarizability tensor to align very slightly with the electric field of the pump pulse. The alignment produces the transient birefringence observed in the experiments. Following the pump pulse, the birefringence decays as the structures randomize with the slowest time constant, t_3 . For t_3 to result from proton hopping, the pump pulse electric field would need to induce anisotropic proton hopping. Protons would have to hop to Hbonded water molecules in a preferential direction to produce birefringence. The OHD-OKE measurements of HCl, NaCl, and LiCl are different in their details, but the qualitative nature of the signals is similar. The fast decays $(t_1 \text{ and } t_2)$ in HCl are not related to proton hopping, as seen from their IMF dependence in Figure 2, but they are very similar to those in NaCl and LiCl. 48 For the t_3 of the HCl solutions to be caused by proton hopping, it would be necessary for the birefringences caused by fast and slow relaxations to be generated by entirely different mechanisms. In contrast, in chloride salts, the fast and slow relaxations are caused by the same mechanism, the coupling of the pump pulse electric field to the ion/water structural relaxation. Comparison to the NaCl and LiCl data shows that it would be unphysical for the HCl signal decaying with time constant t_3 to be caused by proton hopping alone; instead, the comparison supports the mechanism that t_3 is a measure of structural relaxation.

The linear dependence of the bulk viscosity on t_3 also supports the mechanism that t_3 structural evolution is responsible for both the viscosity and proton hopping. Theoretical descriptions of liquid viscosity vary, 72 but they generally involve thermal equilibrium structural fluctuations. In the Eyring theory of viscosity, 73 in a single component molecular liquid under thermal equilibrium conditions, molecules randomly exchange places via rotations and translations, which is spatially isotropic. This process is a type of molecular random walk. The molecular exchange is no longer random under an externally applied force, e.g., gravity. The random walk becomes biased in the direction of the force, resulting in net flow. In the hydronium/chloride/water solutions, there are no identical molecules undergoing a biased walk upon application of a force. In analogy to a simple molecular liquid, the viscosity will be determined by a force causing a directional bias in the structural relaxation of local ion/water clusters, resulting in a net flow. In this picture, the viscosity is linearly dependent on t_3 because t_3 is the cluster structural relaxation time, and the structural relaxation becomes directionally biased under the application of a force. For viscosity to be dependent solely on proton hopping, it would be necessary for an externally applied force, such as gravity, to produce anisotropic proton hopping. Further,

proton hopping is responsible for fast proton diffusion through the relay mechanism. The mechanism specifically involves proton diffusion without physical diffusion of the hydronium cations (vehicular mechanism).

Based on the arguments given above, we conclude that structural relaxation of local hydronium/chloride/water clusters with the time constant t_3 generates potential fluctuations of hydronium hydrogens that are responsible for proton hopping. These same cluster structural fluctuations enable translational diffusion and directional translation under the application of a force. Then, both changes in proton hopping and the bulk viscosity have the same cause, the structural relaxation with time constant t_3 .

A reasonable question is why does the concentration-dependent viscosity track the concentration dependence of the slowest time constant for HCl while the viscosities in the salt solutions track the correlation times? Although we cannot answer this question now, there are two significant differences between salt and HCl solutions. All salt solutions studied have monatomic cations, while the HCl has a polyatomic hydronium cation. To the best of our knowledge, the five salt studies and this HCl study are the only ones that have examined relationships between the bulk viscosities and slow components of the picosecond time scale structural relaxation. The relationship between the bulk viscosity and the structural relaxation of salts with polyatomic cations remains an open question.

The fundamental difference between the hydronium cation and monatomic and polyatomic salt solution cations may be more critical. The slowest relaxation in the salt solutions involves the translation of ions and orientational changes of ion clusters. In addition to these processes, another structural change occurs in HCl solutions. Consider a hydronium⁺/Cl⁻ contact ion pair. The relaxation with time constant t_3 modulates the potential, inducing a proton to hop. The Cl-, which was paired with the hydronium cation with a strong electrostatic interaction, is suddenly solvated by a neutral water molecule with a different hydroxyl configuration. The protonaccepting water, which may have been weakly H-bonded to a Cl⁻, is suddenly a cation with three rather than two hydroxyls. In contrast to the salt solutions, structural fluctuations cause an evolution of the structure and induce sudden structural changes. This change in the location of the positive charge will drive relaxation to new configurations. This difference between the structural relaxations of salt and HCl solutions might be responsible for the different relationships between their microscopic dynamics and the bulk viscosity. Studies of salts with polyatomic cations and other acids should clarify the relationships between the bulk viscosities and structural dynamics.

■ IV. CONCLUDING REMARKS

We have presented a detailed study of the structural dynamics of HCl from a moderate to very high concentration. The most important aspects of this work involve the slow structural dynamics, characterized by the time constant t_3 . Simulations of HCl and comparisons of prior LiCl experimental results and LiCl simulations support the assignment of t_3 to the structural relaxation of hydronium/chloride/water clusters. At moderately high through very high concentrations, there is an insufficient number of water molecules to solvate and separate these clusters. Therefore, the solution will form extended hydronium/chloride/water networks.

The structural relaxation of hydronium/chloride/water clusters with concentration-dependent time constant t_3 governs important properties of HCl solutions, both microscopic and macroscopic. We found that the bulk viscosity is linearly dependent on t_3 (see Figure 7). The extended network is composed of local clusters with a variety of structures. The relaxation of the local structures requires random orientational and translational motions. With the application of a directional force such as gravity, the motions are no longer random and the result is flow. As cluster relaxation slows with increasing concentration, the viscosity increases linearly with the relaxation time. The concentration dependence of the slow time scale structural relaxation is responsible for the concentration dependence of bulk viscosity.

The results also indicate that the cluster structural relaxation governs the proton hopping time. The concentration dependencies (IMF) of t_3 and the simulated and measured proton hopping time fall on the same line (see Figure 8). Although the experimental and simulated hopping data are limited, this correlation of t_3 with the proton hopping times shows that the cluster structural relaxation gives rise to the hydroxyl hydrogens' potential fluctuations that induce proton hopping. As the concentration increases, the hydronium/chloride/water cluster relaxation, with time constant t_3 , becomes slower and proton hopping tracks this slowing. The net result of the experiments and analysis is that in moderate to highly concentrated HCl solutions, the slowest component of the dynamics, i.e., cluster dynamics, underpins important macroscopic and microscopic properties.

ASSOCIATED CONTENT

Data Availability Statement

Data are available by contacting Professor Michael D. Fayer Department of Chemistry Stanford University Stanford, CA 94305–5080 email: fayer@stanford.edu

Supporting Information

The Supporting Information is available free of charge at https://pubs.acs.org/doi/10.1021/jacs.3c11620.

Complete sets of OHD-OKE decays of both NaCl and HCl solutions and different concentrations; individual amplitudes of all exponential fit components; viscosity of HCl solutions as a function of an acid concentration and the correlation time representing the slow dynamics, $\tau_{\rm C}^{\rm slow} = C_3 t_3$, from OHD-OKE measurements (PDF)

AUTHOR INFORMATION

Corresponding Author

Michael D. Fayer — Department of Chemistry, Stanford University, Stanford, California 94305, United States; orcid.org/0000-0002-0021-1815; Phone: 650 723-4446; Email: fayer@stanford.edu

Authors

Laura Kacenauskaite – Department of Chemistry, Stanford University, Stanford, California 94305, United States; Nano-Science Center & Department of Chemistry, University of Copenhagen, Copenhagen 2100, Denmark

Max Moncada Cohen — Department of Chemistry, Stanford University, Stanford, California 94305, United States; orcid.org/0000-0003-1633-6732

Article

Stephen J. Van Wyck — Department of Chemistry, Stanford University, Stanford, California 9430S, United States;
orcid.org/0000-0001-9011-9977

Complete contact information is available at: https://pubs.acs.org/10.1021/jacs.3c11620

Notes

The authors declare no competing financial interest.

ACKNOWLEDGMENTS

This work was supported by the National Science Foundation, Division of Chemistry, award number 2319637. L.K. acknowledges the support of Villum Fonden (project no. 41380). M.M.C. gratefully acknowledges the support of the Weldon G. Brown Fellowship.

■ REFERENCES

- (1) Roy, S.; Schenter, G. K.; Napoli, J. A.; Baer, M. D.; Markland, T. E.; Mundy, C. J. Resolving Heterogeneous Dynamics of Excess Protons in Aqueous Solution with Rate Theory. *J. Phys. Chem. B* **2020**, *124*, 5665–5675.
- (2) Gutman, M.; Nachliel, E. Time-resolved Dynamics of Proton Transfer in Proteinous Systems. *Annu. Rev. Phys. Chem.* **1997**, 48, 329–356.
- (3) Suarez, S. N.; Jayakody, J. R. P.; Greenbaum, S. G.; Zawodzinski, T., Jr.; Fontanella, J. J. A Fundamental Study of the Transport Properties of Aqueous Superacid Solutions. *J. Phys. Chem. B* **2010**, *114*, 8941–8947.
- (4) Ali, I.; Gupta, V. K. Advances in water treatment by adsorption technology. *Nat. Protoc.* **2006**, *1*, 2661–2667.
- (5) Nikoloski, A. N.; Ang, K.-L. Review of the Application of Ion Exchange Resins for the Recovery of Platinum-Group Metals From Hydrochloric Acid Solutions. *Miner. Process. Extr. Metall. Rev.* **2014**, 35, 369–389.
- (6) Ahmed, I.; Summers, J. K.; Promising Techniques for Wastewater Treatment and Water Quality Assessment. *BoD–Books on Demand* 2021, ISBN 978–971–83881–83901–83889.
- (7) Chen, W. S.; Liu, W. S.; Chen, W. C. Leaching Efficiency and Kinetics of Platinum from Spent Proton Exchange Membrane Fuel Cells by $\rm H_2O_2/HCl.$ Metals 2023, 13, 1006.
- (8) Schuster, M.; Kreuer, K.-D.; Steininger, H.; Maier, J. Proton conductivity and diffusion study of molten phosphonic acid H₃PO₃. *Solid State Ion.* **2008**, *179*, 523–528.
- (9) Knight, C.; Voth, G. A. The Curious Case of the Hydrated Proton. Acc. Chem. Res. 2012, 45, 101–109.
- (10) Brünig, F. N.; Rammler, M.; Adams, E. M.; Havenith, M.; Netz, R. R. Spectral signatures of excess-proton waiting and transfer-path dynamics in aqueous hydrochloric acid solutions. *Nat. Commun.* **2022**, *13*, 4210.
- (11) Fournier, J. A.; Carpenter, W. B.; Lewis, N. H. C.; Tokmakoff, A. Broadband 2D IR spectroscopy reveals dominant asymmetric $H_5O_2^+$ proton hydration structures in acid solutions. *Nat. Chem.* **2018**, 10. 932–937.
- (12) Li, X.-Y.; Wang, T.; Cai, Y.-C.; Meng, Z.-D.; Nan, J.-W.; Ye, J.-Y.; Yi, J.; Zhan, D.-P.; Tian, N.; Zhou, Z.-Y.; Sun, S.-G. Mechanism of Cations Suppressing Proton Diffusion Kinetics for Electrocatalysis. *Angew. Chem., Int. Ed.* **2023**, *62*, No. e202218669.
- (13) Fischer, S. A.; Dunlap, B. I.; Gunlycke, D. Correlated dynamics in aqueous proton diffusion. *Chem. Sci.* **2018**, *9*, 7126–7132.
- (14) Agmon, N. The Grotthuss mechanism. Chem. Phys. Lett. 1995, 244, 456–462.
- (15) Mabuchi, T. Revealing the Anticorrelation Behavior Mechanism between the Grotthuss and Vehicular Diffusions for Proton Transport in Concentrated Acid Solutions. *J. Phys. Chem. B* **2022**, *126*, 3319–3326.

- (16) De Grotthuss, C. Memoir on the decomposition of water and of the bodies that it holds in solution by means of galvanic electricity. *Biochim. Biophys. Acta Bioenerg.* **2006**, *1757*, 871–875.
- (17) Arntsen, C.; Chen, C.; Calio, P. B.; Li, C.; Voth, G. A. The hopping mechanism of the hydrated excess proton and its contribution to proton diffusion in water. *Int. J. Chem. Phys.* **2021**, *154*, No. 194506.
- (18) Hynes, J. T. The protean proton in water. *Nature* **1999**, 397, 565–567.
- (19) Day, T. J. F.; Schmitt, U. W.; Voth, G. A. The Mechanism of Hydrated Proton Transport in Water. J. Am. Chem. Soc. 2000, 122, 12027–12028.
- (20) Meiboom, S. Nuclear Magnetic Resonance Study of the Proton Transfer in Water. *Int. J. Chem. Phys.* **2004**, *34*, 375–388.
- (21) Marx, D.; Tuckerman, M. E.; Hutter, J.; Parrinello, M. The nature of the hydrated excess proton in water. *Nature* **1999**, 397, 601–604.
- (22) Geissler, P. L.; Dellago, C.; Chandler, D.; Hutter, J.; Parrinello, M. Autoionization in Liquid Water. *Science* **2001**, *291*, 2121–2124.
- (23) Dahms, F.; Fingerhut, B. P.; Nibbering, E. T. J.; Pines, E.; Elsaesser, T. Large-amplitude transfer motion of hydrated excess protons mapped by ultrafast 2D IR spectroscopy. *Science* **2017**, 357, 491–495.
- (24) Kim, J.; Schmitt, U. W.; Gruetzmacher, J. A.; Voth, G. A.; Scherer, N. E. The vibrational spectrum of the hydrated proton: Comparison of experiment, simulation, and normal mode analysis. *Int. J. Chem. Phys.* **2002**, *116*, 737–746.
- (25) Fulton, J. L.; Balasubramanian, M. Structure of Hydronium (H_3O^+) /Chloride (Cl^-) Contact Ion Pairs in Aqueous Hydrochloric Acid Solution: A Zundel-like Local Configuration. *J. Am. Chem. Soc.* **2010**, *132*, 12597–12604.
- (26) Kazmierczak, L.; Janik, I.; Wolszczak, M.; Swiatla-Wojcik, D. Dynamics of Ion Pairing in Dilute Aqueous HCl Solutions by Spectroscopic Measurements of Hydroxyl Radical Conversion into Dichloride Radical Anions. J. Phys. Chem. B 2021, 125, 9564–9571.
- (27) Yuan, R.; Napoli, J. A.; Yan, C.; Marsalek, O.; Markland, T. E.; Fayer, M. D. Tracking Aqueous Proton Transfer by Two-Dimensional Infrared Spectroscopy and *ab initio* Molecular Dynamics Simulations. *ACS Cent. Sci.* **2019**, *5*, 1269–1277.
- (28) Thämer, M.; De Marco, L.; Ramasesha, K.; Mandal, A.; Tokmakoff, A. Ultrafast 2D IR spectroscopy of the excess proton in liquid water. *Science* **2015**, *350*, 78–82.
- (29) Carpenter, W. B.; Fournier, J. A.; Lewis, N. H. C.; Tokmakoff, A. Picosecond Proton Transfer Kinetics in Water Revealed with Ultrafast IR Spectroscopy. *J. Phys. Chem. B* **2018**, 122, 2792–2802.
- (30) Ando, K.; Hynes, J. T. Molecular Mechanism of HCl Acid Ionization in Water: *ab initio* Potential Energy Surfaces and Monte Carlo Simulations. *J. Phys. Chem. B* **1997**, *101*, 10464–10478.
- (31) Heuft, J. M.; Meijer, E. J. A density functional theory based study of the microscopic structure and dynamics of aqueous HCl solutions. *Phys. Chem. Chem. Phys.* **2006**, *8*, 3116–3123.
- (32) Kollman, P.; Johansson, A.; Rothenberg, S. HCl and HF proton donors: a theoretical study. *Chem. Phys. Lett.* **1974**, *24*, 199–202.
- (33) Farrell, K. M.; Zanni, M. T. Observing Aqueous Proton Transfer Dynamics. ACS Cent. Sci. 2019, 5, 1114–1116.
- (34) Bertagnolli, H.; Chieux, P.; Hertz, H. G. Absence of fast H⁺-ion motion in aqueous HCl. A neutron scattering study. *J. Chem. Soc., Faraday Trans.* 1 1987, 1 (83), 687–695.
- (35) Botti, A.; Bruni, F.; Imberti, S.; Ricci, M. A.; Soper, A. K. Ions in water: The microscopic structure of a concentrated HCl solution. *Int. J. Chem. Phys.* **2004**, *121*, 7840–7848.
- (36) Sahle, C. J.; Niskanen, J.; Schmidt, C.; Stefanski, J.; Gilmore, K.; Forov, Y.; Jahn, S.; Wilke, M.; Sternemann, C. Cation Hydration in Supercritical NaOH and HCl Aqueous Solutions. *J. Phys. Chem. B* **2017**, *121*, 11383–11389.
- (37) Dahms, F.; Costard, R.; Pines, E.; Fingerhut, B. P.; Nibbering, E. T. J.; Elsaesser, T. The Hydrated Excess Proton in the Zundel Cation ${\rm H_5O_2}^+$: The Role of Ultrafast Solvent Fluctuations. *Angew. Chem., Int. Ed.* **2016**, *55*, 10600–10605.

- (38) Schwaab, G.; Sebastiani, F.; Havenith, M. Ion Hydration and Ion Pairing as Probed by THz Spectroscopy. *Angew. Chem., Int. Ed.* **2019**, *58*, 3000–3013.
- (39) Decka, D.; Schwaab, G.; Havenith, M. A THz/FTIR fingerprint of the solvated proton: evidence for Eigen structure and Zundel dynamics. *Phys. Chem. Chem. Phys.* **2015**, *17*, 11898–11907.
- (40) Maiorov, V. D.; Kislina, I. S.; Rykounov, A. A.; Vener, M. V. The structure and vibrational features of proton disolvates in water—ethanol solutions of HCl: the combined spectroscopic and theoretical study. *J. Phys. Org. Chem.* **2014**, *27*, 135–141.
- (41) Baer, M. D.; Fulton, J. L.; Balasubramanian, M.; Schenter, G. K.; Mundy, C. J. Persistent Ion Pairing in Aqueous Hydrochloric Acid. *J. Phys. Chem. B* **2014**, *118*, 7211–7220.
- (42) Desbat, B.; Huong, P. V. Determination by Raman spectroscopy of the solvation number of the chloride ion in liquid hydrogen chloride. *J. Raman Spectrosc.* **1979**, *8*, 177–179.
- (43) Kemp, D. D.; Gordon, M. S. Theoretical Study of the Solvation of Fluorine and Chlorine Anions by Water. *J. Phys. Chem. A* **2005**, 109, 7688–7699.
- (44) Bresnahan, C. G.; David, R.; Milet, A.; Kumar, R. Ion Pairing in HCl–Water Clusters: From Electronic Structure Investigations to Multiconfigurational Force-Field Development. *J. Phys. Chem. A* **2019**, *123*, 9371–9381.
- (45) Foggi, P.; Bellini, M.; Kien, D. P.; Vercuque, I.; Righini, R. Relaxation Dynamics of Water and HCl Aqueous Solutions Measured by Time-Resolved Optical Kerr Effect. *J. Phys. Chem. A* **1997**, *101*, 7029–7035.
- (46) Santa, I.; Foggi, P.; Righini, R.; Williams, J. H. Time-Resolved Optical Kerr Effect Measurements in Aqueous Ionic Solutions. *J. Phys. Chem.* **1994**, *98*, 7692–7701.
- (47) Palese, S.; Schilling, L.; Miller, R. J. D.; Staver, P. R.; Lotshaw, W. T. Femtosecond optical Kerr effect studies of water. *J. Phys. Chem.* **1994**, *98*, *6308–6316*.
- (48) Van Wyck, S. J.; Fayer, M. D. Dynamics of Concentrated Aqueous Lithium Chloride Solutions Investigated with Optical Kerr Effect Experiments. *J. Phys. Chem. B* **2023**, *127*, 3488–3495.
- (49) Singh, M. B.; Dalvi, V. H.; Gaikar, V. G. Investigations of Clustering of Ions and Diffusivity in Concentrated Aqueous Solutions of Lithium Chloride by Molecular Dynamic Simulations. *RSC Adv.* **2015**, *5*, 15328–15337.
- (50) Nishikata, E.; Ishii, T.; Ohta, T. Viscosities of aqueous hydrochloric acid solutions, and densities and viscosities of aqueous hydroiodic acid solutions. *J. Chem. amp; Eng. Data* **1981**, 26, 254–256.
- (51) Ozbek, H. Viscosity of aqueous sodium chloride solutions from 0-150 °C.; Lawrence Berkeley National Laboratory 1971, https://escholarship.org/uc/item/3jp6n2bf.
- (52) Deeg, F. W.; Stankus, J. J.; Greenfield, S. R.; Newell, V. J.; Fayer, M. D. Anisotropic Reorientational Relaxation of Biphenyl: Transient Grating Optical Kerr Effect Measurements. *Int. J. Chem. Phys.* **1989**, *90*, 6893–6902.
- (53) Ruhman, S.; Williams, L. R.; Joly, A. G.; Kohler, B.; Nelson, K. A. Nonrelaxational Inertial Motion in Carbon Disulfide Liquid Observed by Femtosecond Time-Resolved Impulsive Stimulated Scattering. *J. Phys. Chem.* **1987**, *91*, 2237–2240.
- (54) Yan, Y. X.; Nelson, K. A. Impulsive Stimulated Light Scattering. I. General Theory. *Int. J. Chem. Phys.* 1987, 87, 6240–6256.
- (55) Fecko, C.; Eaves, J.; Tokmakoff, A. Isotropic and Anisotropic Raman Scattering from Molecular Liquids Measured by Spatially Masked Optical Kerr Effect Spectroscopy. *Int. J. Chem. Phys.* **2002**, *117*, 1139–1154.
- (56) Sha, M.; Yamada, S. A.; Fayer, M. D. Orientational Pair Correlations and Local Structure of Benzonitrile from Molecular Dynamics Simulations with Comparisons to Experiments. *J. Phys. Chem. B* **2021**, *125*, 3163–3177.
- (57) Chandler, D. Introduction to Modern Statistical Mechanics; Oxford University Press: New York, 1987.

- (58) Sturlaugson, A. L.; Arima, A. Y.; Bailey, H. E.; Fayer, M. D. Orientational Dynamics in a Lyotropic Room Temperature Ionic Liquid. *J. Phys. Chem. B* **2013**, *117*, 14775–14784.
- (59) Sturlaugson, A. L.; Fruchey, K. S.; Fayer, M. D. Orientational Dynamics of Room Temperature Ionic Liquid/Water Mixtures: Water-Induced Structure. *J. Phys. Chem. B* **2012**, *116*, 1777–1787.
- (60) Van Wyck, S. J.; Fayer, M. D. Dynamics of Acrylamide Hydrogels, Polymers, and Monomer in Water Measured with Optical Heterodyne Detected Optical Kerr Effect Spectroscopy. *J. Phys. Chem. B* **2023**, *127*, 1276–1286.
- (61) Ge, L.; Bernasconi, L.; Hunt, P. Linking electronic and molecular structure: insight into aqueous chloride solvation. *Phys. Chem. Chem. Phys.* **2013**, *15*, 13169–13183.
- (62) Schröder, M.; Gatti, F.; Lauvergnat, D.; Meyer, H.-D.; Vendrell, O. The coupling of the hydrated proton to its first solvation shell. *Nat. Commun.* **2022**, *13*, 6170.
- (63) Xu, J.; Izvekov, S.; Voth, G. A. Structure and Dynamics of Concentrated Hydrochloric Acid Solutions. *J. Phys. Chem. B* **2010**, 114, 9555–9562.
- (64) Calio, P. B.; Li, C.; Voth, G. A. Molecular Origins of the Barriers to Proton Transport in Acidic Aqueous Solutions. *J. Phys. Chem. B* **2020**, *124*, 8868–8876.
- (65) Wang, X.; Toroz, D.; Kim, S.; Clegg, S. L.; Park, G.-S.; Di Tommaso, D. Density functional theory based molecular dynamics study of solution composition effects on the solvation shell of metal ions. *Phys. Chem. Chem. Phys.* **2020**, 22, 16301–16313.
- (66) Mao, S.; Duan, Z. The Viscosity of Aqueous Alkali-Chloride Solutions up to 623 K, 1,000 bar, and High Ionic Strength. *Int. J. Thermophys.* **2009**, *30*, 1510–1523.
- (67) Kacenauskaite, L.; Van Wyck, S. J.; Cohen, M. M.; Fayer, M. D. Water-in-Salt: Fast Dynamics, Structure, Thermodynamics, and Bulk Properties. *J. Phys. Chem. B* **2024**, *128*, 291.
- (68) De Grotthuss, C. Sur la décomposition de l'eau et des corps qu'elle tient en dissolution à l'aide de l'électricité galvanique. *Ann. Chim.* **1806**, 58, 54.
- (69) Kreuer, K.-D.; Rabenau, A.; Weppner, W. Vehicle Mechanism, A New Model for the Interpretation of the Conductivity of Fast Proton Conductors. *Angew. Chem., Int. Ed. Engl.* 1982, 21, 208–209.
- (70) Asbury, J. B.; Steinel, T.; Stromberg, C.; Corcelli, S.; Lawrence, C.; Skinner, J.; Fayer, M. Water Dynamics: Vibrational Echo Correlation Spectroscopy and Comparison to Molecular Dynamics Simulations. *J. Phys. Chem. A* **2004**, *108*, 1107–1119.
- (71) Asbury, J. B.; Steinel, T.; Kwak, K.; Corcelli, S. A.; Lawrence, C. P.; Skinner, J. L.; Fayer, M. D. Dynamics of Water Probed with Vibrational Echo Correlation Spectroscopy. *J. Chem. Phys.* **2004**, *121*, 12431–12446.
- (72) Rha, C. In *Theory, Determination and Control of Physical Properties of Food Materials*; Rha, C., Ed.; Springer: Netherlands: Dordrecht, 1975; p 7–24.
- (73) Ewell, R. H.; Eyring, H. Theory of the Viscosity of Liquids as a Function of Temperature and Pressure. *Int. J. Chem. Phys.* **2004**, *5*, 726–736.